Molecular Neurobiology (2026) 63:812
https://doi.org/10.1007/s12035-026-06110-5

RESEARCH

Zafirlukast Exacerbates Behavioral Seizure Activity and Blood–Brain Barrier Disruption Despite Modestly Reducing Neuronal Injury Markers in a PTZ-Induced Early Epileptogenesis Mouse Model

Volkan Gorgulu[1,2] · Cansin Sirin Tomruk[2,3] · Pelin Ergun[4,5] · Berrin Ozdil[2,6] · Ebru Sanci[7] · Aylin Buhur[2,8] · Eser Y. Sozmen[9] · Timur Kose[10] · Nefise Ulku Karabay Yavasoglu[11] · Altug Yavasoglu[2]

Received: 8 June 2026 / Accepted: 29 July 2026 / Published online: 5 August 2026

Abstract

Epilepsy is one of the most prevalent neurological disorders worldwide, and approximately 25% of patients remain refractory to pharmacological treatment. Blood–brain barrier (BBB) disruption and reactive gliosis are key mechanisms implicated in early epileptogenesis. This study investigated the effects of zafirlukast, a leukotriene receptor antagonist, on BBB permeability, reactive gliosis, and behavioral seizure activity in a pentylenetetrazol (PTZ)-induced early epileptogenesis model in C57BL/6 mice. Zafirlukast was administered twice daily at a dose of 10 mg/kg. Seizure activity was evaluated by behavioral observation in terms of seizure severity, latency, duration, and frequency. BBB permeability was assessed using the Evans Blue assay, and brain tissues were analyzed by biochemical and immunohistochemical methods. The PTZ + ZAFIR group exhibited more severe seizures, characterized by increased seizure frequency and duration, shorter latency, and a higher kindling rate (80% vs. 27%). BBB permeability was also increased, whereas MMP-9 levels remained, suggesting disruption may be linked to direct mechanical effects of recurrent seizures rather than inflammation. Clues suggest that zafirlukast may exert paradoxical effects on two prominent cell types involved in reactive gliosis. While increased GFAP and TGF-β1 expression may reflect enhanced astrocyte activation, changes in IL-1β and Iba1 expression suggest suppression of microglial activation. Notably, pro-inflammatory and oxidative stress markers remained unchanged despite the increase in seizure severity. The observed reduction in neurodegeneration may be attributable to the suppressive effects of zafirlukast on microglial activation and the subsequent reduction in pro-inflammatory cytokine release. These findings indicate a complex role for leukotriene signaling during early epileptogenesis. Further studies using different doses, vehicles, and experimental models are warranted to clarify the effects of zafirlukast on the mechanisms underlying early epileptogenesis.

Keywords Zafirlukast · Epilepsy · Seizures · Blood–brain barrier · Gliosis · Astrocytes

Introduction

Epilepsy is one of the most common neurological disorders, affecting approximately 50 million people of all ages worldwide [1]. Despite the availability of numerous antiseizure medications and access to well-established healthcare systems, approximately 25% of newly diagnosed patients fail to achieve 1-year seizure freedom despite treatment [2]. This highlights the need for novel therapeutic strategies. Furthermore, according to the International League Against Epilepsy (ILAE), approximately 25% of epilepsy cases are associated with preventable etiologies [3]. These preventable forms of epilepsy often arise following an initial brain insult, such as traumatic brain injury [4]. Following the initial insult, epileptogenesis is initiated, during which the brain acquires the capacity to generate spontaneous seizures [4, 5]. Accordingly, studies of early epileptogenesis are critical for understanding the pathophysiology of epilepsy and for the development of more effective treatments.

Seizures are widely recognized to result from an imbalance between excitatory and inhibitory mechanisms in the brain [6]. Blood–brain barrier (BBB) disruption following the initial brain insult is considered a pivotal event during epileptogenesis [5]. Reactive gliosis contributes to neuronal hyperexcitability and increases seizure susceptibility. Moreover, each seizure may induce further brain injury, creating

Extended author information available on the last page of the article

a self-perpetuating cycle [5, 7]. Interrupting this cycle at an early stage represents a promising therapeutic approach.

Leukotrienes (LTs) are paracrine mediators involved in chemotaxis and the regulation of vascular permeability [8]. Previous studies have primarily focused the role of cysteinyl leukotrienes (Cys-LTs) in epilepsy [9–13] and other neurological disorders [8] suggest that cysteinyl leukotriene receptor (Cys-LTR) antagonists may have therapeutic potential. However, these studies have primarily focused on seizure severity and electrophysiological outcomes, whereas their effects on the histopathological features of reactive gliosis remain largely unexplored. Furthermore, no studies have investigated the effects of Cys-LTR antagonists on blood–brain barrier (BBB) integrity during early epileptogenesis. Among Cys-LTR antagonists, montelukast has been the most extensively investigated under epileptic conditions. In contrast, zafirlukast, a Cys-LTR antagonist, despite its distinct chemical and pharmacological properties, has not been evaluated in any experimental model of epilepsy. Notably, zafirlukast has been shown to attenuate inflammatory responses and reduce BBB permeability in an experimental model of ischemic brain injury [14]. The present study was designed to address this knowledge gap and to determine whether the previously reported antiepileptic and neuroprotective effects of montelukast represent a class effect of Cys-LTR antagonists or are specific to montelukast. We hypothesized that zafirlukast would attenuate behavioral seizure activity, preserve blood–brain barrier integrity, and reduce reactive gliosis during early epileptogenesis. Accordingly, we investigated the effects of zafirlukast on behavioral seizure activity, BBB permeability, and reactive gliosis in a pentylenetetrazole (PTZ)-induced model of early epileptogenesis in C57BL/6 mice.

Materials and Methods

Animal Welfare and Drug Preparations

The study was approved by the Ege University Animal Experiments Local Ethics Committee (Approval No. 2020-119). All experimental procedures were conducted in accordance with the ARRIVE 2.0 guidelines. A total of 75 male C57BL/6 mice (20–25 g) (Kobay AŞ, Ankara, Türkiye) were used. The animals were housed at the Ege University Drug Development and Pharmacokinetic Research and Application Center (ARGEFAR) under a 12-h light/dark cycle, with food and water available ad libitum. Following a 1-week acclimatization period, early epileptogenesis was induced using a subconvulsive dose of pentylenetetrazole (PTZ; 35 mg/kg) (P6500, Sigma-Aldrich, St. Louis, MO, USA). PTZ was dissolved in 0.9% saline at a concentration of 2 mg/mL [15]. Zafirlukast (10008282, Cayman Chemical, Ann Arbor, MI, USA) was initially dissolved in dimethyl sulfoxide (DMSO) (D2438, Sigma-Aldrich, St. Louis, MO, USA) at a volume of 0.16 mL/kg and subsequently diluted with 0.9% saline to prepare a 1% suspension [14]. All injections were administered using 30G insulin syringes (BD Micro-Fine Plus, Becton, Dickinson and Company, Franklin Lakes, NJ, USA), with injection sites alternated between the left and right lower abdominal quadrants.

Study Design

The animals were stratified by body weight and randomly allocated to five experimental groups ($n = 15$ per group) via Microsoft Excel (Microsoft Corporation, Redmond, WA, USA) by a blinded researcher. Baseline body weight did not differ significantly among the groups (one-way ANOVA, $F = 0.138$, $p = 0.968$). The experimental design is illustrated in Fig. 1.

Experimental groups:

1 -SALINE: 0.9% NaCl was administered i.p. every other day.
2 -DMSO: 1% DMSO was administered i.p. twice a day.
3 -ZAFIR: 10 mg/kg zafirlukast in %1 DMSO suspension was administered i.p. twice daily.
4 -PTZ: 35 mg/kg PTZ was administered i.p. every other day.
5 -PTZ + ZAFIR: 10 mg/kg zafirlukast was administered i.p. twice daily and 35 mg/kg PTZ was administered i.p. every other day.

Seizure Monitoring

Immediately after PTZ administration, each mouse was placed individually in a Plexiglas cage for seizure monitoring. Behavioral seizure activity was recorded using a tripod-mounted mobile camera until complete behavioral recovery. Seizures were evaluated according to the Modified Racine Scale [15, 16]. The behavioral seizure scores were defined as follows: Score 0, no behavioral changes; Score 1, immobility and lying prone; Score 2, head nodding, facial myoclonus, and partial myoclonus; Score 3, whole-body myoclonus and tail elevation; Score 4, forelimb clonus, rearing, and falling to the side; Score 5, generalized tonic–clonic seizures, wild running, and falling backward; Score 6, death. Mice exhibiting three consecutive seizures with a score of ≥4 were considered fully kindled [17, 18]. Seizure score, latency (time from PTZ administration to the onset of the first myoclonic event), duration (total duration of score 4–5 seizures during a single observation period), and frequency (number of score 4–5 seizures per observation period) were analyzed from video recordings by a researcher blinded to the experimental

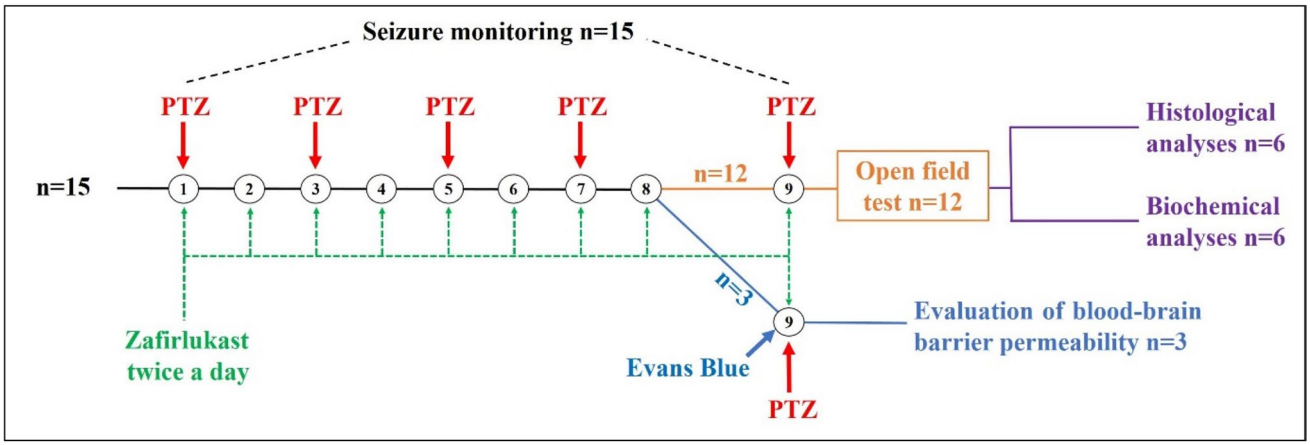

Fig. 1 Flow diagram of experiments. Numbers in round boxes represent days. PTZ, pentylenetetrazole

groups. The seizure monitoring protocol was terminated on day 9.

Open Field Test

The open field maze test was performed in a square arena (50 × 50 × 38 cm) made of gray-painted wood [19, 20]. The floor of the arena was divided into equal 10 × 10 cm squares to facilitate behavioral analysis [19]. Illumination at the floor level was maintained at 100 ± 5 lx, as measured using a lux meter (Supplementary Fig. 1) [21]. Twelve mice from each group underwent the open field test one day after the final PTZ injection. Between trials, the arena was cleaned with 95% ethanol and allowed to dry for 10 min to eliminate olfactory cues. Each mouse was placed in the center of the arena, and behavior was recorded for 10 min using a tripod-mounted camera. At the end of each session, the number of fecal boli was recorded. Movement trajectories were analyzed using ANY-maze software version 7.2 (Stoelting Europe, Dublin, Ireland). The total distance traveled, average speed, time spent in the center zone, and heat map distributions were quantified.

Evaluation of Blood Brain Barrier Permeability

Three mice from each group were included in the BBB permeability assessment. Evans Blue dye (E2129, Sigma-Aldrich, St. Louis, MO, USA) was prepared as a 2% solution (20 mg/mL) in phosphate-buffered saline (PBS). A volume of 0.1 mL was administered via the tail vein 1 h before the final PTZ injection [22]. Successful systemic distribution of the dye was verified by visible staining of peripheral tissues, including the ears, nose, extremities, and torso (Supplementary Fig. 2 A). After 1 h of circulation, PTZ was administered, and behavioral seizure activity was monitored until complete recovery. General anesthesia was subsequently induced using ketamine hydrochloride (80 mg/kg) and xylazine hydrochloride (5 mg/kg). The thoracic cavity was opened (Supplementary Fig. 2B), and transcardial perfusion was performed through the left ventricle using a 24G intravenous cannula. Circulating Evans Blue dye was removed by perfusion with 25–50 mL of 0.9% saline, while an incision was made in the right atrium to facilitate drainage [22]. After clear perfusate was observed from the right atrium, fixation was performed using 4% paraformaldehyde (PFA) in PBS (Supplementary Fig. 2 C). The brains were then rapidly removed and post-fixed in 4% PFA in PBS for 48 h. Tissues were cryoprotected in 15% sucrose in PBS at 4 °C until they sank completely, followed by incubation in 30% sucrose in PBS overnight at 4 °C. Subsequently, tissues were embedded in optimal cutting temperature (OCT) compound (Tissue-Tek Sakura, California, USA) and rapidly frozen in liquid nitrogen vapor. Frozen tissue blocks were stored at −80 °C in sealed containers until sectioning. Coronal brain sections (15 µm thickness) were obtained using a cryostat (CRYO-CUT, American Optical Corporation, USA) at −20 °C and mounted onto glass slides. Cryosections were stored at −20 °C in sealed slide boxes until further processing. On the day of imaging, sections were equilibrated to room temperature and coverslipped using a DAPI-containing mounting medium (1214, BioVision, California, USA).

Histological Preparations

Six animals from each group were included in the histological analyses one day after completion of the open field test. Under the general anesthesia transcardial perfusion was performed using 4% PFA in PBS. Following perfusion, brains were rapidly removed and post-fixed in 4% PFA in PBS for 48 h. Subsequently, tissues were dehydrated through a graded series of ethanol, cleared in xylene, and embedded in paraffin blocks. Serial Sects. (5 µm thickness)

were obtained using a microtome (Leica RM 2145, Illinois, USA). Hematoxylin–eosin (H&E) (05–06004/L, Bio-Optica, Milano, Italy; RRSP35/E, Atom Scientific, Manchester, UK) and Cresyl violet (05-B16001, Bio-Optica, Milano, Italy) staining methods were conducted to evaluate general tissue morphology.

Immunohistochemical Staining

Antigen retrieval was performed with sodium citrate in the microwave for 30 min. The sections were then exposed to 1% Triton X solution for 5 min and 3% hydrogen peroxide for 10 min, respectively. Serum blocking (SensiTek HRP Anti-Polyvalent Lab Pack, Scytek, Utah, USA) was then performed for 30 min. Anti-glial fibrillary acidic protein (GFAP), anti-neuronal nuclei (NeuN), anti-ionized calcium-binding adapter molecule-1 (Iba1), anti-mouse serum albumin primary antibodies (respectively bs-0199R, bs-1613R, bs-1363R, bs-2256R, Bioss, Massachusetts, USA) at 1:100 dilution were incubated overnight at +4 °C. The next day, biotinylated secondary antibody (SensiTek HRP Anti-Polyvalent Lab Pack, Scytek, Utah, USA) and streptavidin/horseradish peroxidase (SensiTek HRP Anti-Polyvalent Lab Pack, Scytek, Utah, USA) were applied for 30 min each. After adding 3,3′-diaminobenzidine (DAB) substrate (11718096001, Sigma-Aldrich, St. Louis, USA), counterstaining was performed with Mayer's hematoxylin (05–06002/L, Bio-Optica, Milano, Italy).

Imaging Process

Five brain regions, including the dentate gyrus (DG), cornu ammonis 1 (CA1), cornu ammonis 3 (CA3), cerebral cortex (CC), and cerebellum (CB), were evaluated. All images were acquired using CellSense Entry 1.7.1 software (Olympus, Tokyo, Japan) with the same fluorescence-equipped light microscope (Olympus BX51, Tokyo, Japan) and camera system (Olympus DP72, Tokyo, Japan) under identical acquisition settings for all groups. Image processing and quantitative analyses were performed using ImageJ software (version 1.54f). To quantify Evans Blue fluorescence intensity, images were acquired at 200× magnification from 10 different sections per mouse using identical fluorescence microscope settings across all experimental groups (Supplementary Fig. 3 A). Evans Blue images were converted to 8-bit format and analyzed in the red channel (Supplementary Fig. 3B,C). Fluorescence intensity was quantified using identical threshold values for all groups (Supplementary Fig. 3D). Degenerated neurons were counted in 10 sections per mouse using H&E and Cresyl Violet staining at 400× magnification. Immunohistochemical staining images were acquired at 1000× magnification (10 sections per mouse). Color deconvolution was initially performed on the original images (Supplementary Fig. 4A–C), followed by quantification of DAB staining intensity using identical threshold values across all groups (Supplementary Fig. 4D). All measurements were performed by a researcher blinded to the experimental groups.

Biochemical Analyses

Six mice from each group were euthanized by decapitation using a guillotine one day after the open field test. The brains were rapidly removed, weighed, immediately frozen on dry ice during dissection, and subsequently stored at −80 °C in sealed containers until analysis. On the day of biochemical analysis, brain tissues were thawed at room temperature. The tissues were dissected at the level of the tentorium cerebelli and separated into the cerebrum and cerebellum–brainstem regions. PBS buffer (50 mM, pH 7.4) was added at a ratio of 10 mL per gram of tissue, and samples were homogenized using an automated homogenizer until complete disruption was achieved. The homogenates were centrifuged at 10,000 rpm for 15 min at 4 °C, and the supernatants were collected for further analyses. The levels of interleukin-1β (IL-1β; CSB-E08054m, CUSABIO, Texas, USA), matrix metalloproteinase-9 (MMP-9; CSB-E08007m, CUSABIO, Texas, USA), and transforming growth factor-β1 (TGF-β1; CSB-E04726m, CUSABIO, Texas, USA) were measured using enzyme-linked immunosorbent assay (ELISA) kits according to the manufacturer's instructions. Absorbance values were measured using a microplate reader (Thermo Varioskan Flash, Massachusetts, USA). Cytokine concentrations were normalized to total protein content and expressed per milligram of protein. Total protein concentration was determined using the Lowry method [23].

For malondialdehyde (MDA) analysis, thiobarbituric acid (TBA) reagent was added to the supernatants, followed by incubation at 100 °C for 20 min. Samples were then centrifuged at 2000 rpm for 10 min, and absorbance was measured at 532 nm. MDA levels were calculated from a standard curve generated using 1,1,1,2,3-tetraethoxypropane and expressed as nmol/mL of thiobarbituric acid reactive substances. For myeloperoxidase (MPO) analysis, homogenate samples were diluted 1:10 with PBS. Subsequently, 270 µL of o-dianisidine was added to 30 µL of homogenate, and absorbance was recorded at 460 nm for 10 min. MPO activity was calculated from a standard curve generated using MPO enzyme standards and expressed as U/mg.

Statistical Analysis

The similarity of changes in behavioral seizure activity over the nine-day PTZ induction period between the PTZ and PTZ + ZAFIR groups was evaluated using the nonparametric Brunner–Langer model (F1-LD-F1 design). Relative

treatment effects were used for the graphical presentation of Brunner–Langer analyses. Pairwise time-point comparisons were performed using the same model, and *p*-values were adjusted using the Benjamini–Hochberg correction. Evans Blue permeability, open field test, histological, and biochemical data were analyzed using analysis of variance (ANOVA) or the Kruskal–Wallis test, as appropriate. The experimental unit was defined as a single animal. For histological analyses, the arithmetic mean of 10 measurements obtained from each animal was used for statistical evaluation. Homogeneity of variance was assessed using Levene's test. When the assumption of variance homogeneity was violated, Welch's test was applied. For datasets meeting the assumption of equal variances, Bonferroni post hoc correction was used; otherwise, the Dunnett T3 post hoc test was applied. Following the Kruskal–Wallis test, pairwise comparisons were performed using the Mann–Whitney *U* test with Bonferroni correction. The proportion of fully kindled animals in the PTZ and PTZ + ZAFIR groups was compared using Pearson's chi-square test. Statistical significance was set at $p < 0.05$. All statistical analyses were performed using R software (version 4.0.5; arsenal package, R Foundation for Statistical Computing, Vienna, Austria; http://r-project.org) and SAS software (version 9.3; PROC MIXED procedure, SAS Institute, Cary, NC, USA).

For the four seizure parameters (modified Racine score, latency, frequency, and duration), the effect size of the group main effect was expressed as partial eta-squared (partial η^2), calculated as $(F \times df1)/(F \times df1 + df2)$, using the *F* statistic and degrees of freedom obtained from the ANOVA-type statistic with box-type approximation. For outcomes assessed by one-way ANOVA, effect size was expressed with the bias-corrected omega-squared (ω^2, fixed-effect model), which provides a less inflated estimate of effect size in small samples. For outcomes assessed by the Kruskal–Wallis test, the nonparametric analogue eta-squared (η^2) was used. Confidence intervals for Kruskal–Wallis test effect sizes are not reported, as the standard noncentral-F-based interval estimation is unstable and uninformative at these group sizes.

During the PTZ induction phase, only one animal died, which was in the PTZ + ZAFIR group on the last injection of day 9. Consequently, this animal was not included in the subsequent open field test. Additionally, one animal from the SALINE group was excluded from the open field test due to a lack of proper adaptation to the arena (exhibiting extreme aggression). For biochemical analyses, some animals were excluded from specific ELISA measurements due to technical limitations (e.g., suboptimal measurement conditions or insufficient sample volume). Specifically, one animal from the SALINE group was excluded from the cerebellum–brainstem IL-1β analysis, one animal from the PTZ group from the cerebellum–brainstem MMP-9 analysis, and one animal from the ZAFIR group from the cerebral TGF-β1 analysis. The sample sizes (n values) for each experiment are provided in Supplementary Files 1–10.

Results

Seizure Parameters

Relative treatment effects with 95% confidence intervals for the seizure parameters are presented in Fig. 2A. Zafirlukast markedly accelerated kindling progression. A significantly greater proportion of animals in the PTZ + ZAFIR group developed full kindling (80%) compared with the PTZ group (27%) (Pearson's $\chi^2 = 8.571$, $p = 0.003$). Notably, most animals in the PTZ + ZAFIR group reached full kindling by the fifth PTZ injection. Descriptive statistics, pairwise time-point comparisons, relative treatment effects (RTEs), partial effect sizes (η^2), and 95% confidence intervals are provided in Supplementary Tables 1–10 (Supplementary File 1).

Seizure severity was consistently greater in the PTZ + ZAFIR group than in the PTZ group throughout the experimental period ($p < 0.001$) (Fig. 2B). Both groups exhibited a similar pattern of increase in modified Racine scores over the 9-day period (group × time interaction, $p = 0.960$). However, the temporal increase was significant within each group ($p < 0.001$). Latency to the first myoclonic event was significantly shorter in the PTZ + ZAFIR group than in the PTZ group ($p = 0.019$). The temporal change in latency over the 9-day period was similar between the groups ($p = 0.651$), whereas significant within-group changes were observed in both groups ($p = 0.008$).

Seizure frequency (score ≥ 4) was significantly higher in the PTZ + ZAFIR group than in the PTZ group throughout the study period ($p < 0.001$). Both groups exhibited a similar temporal increase in seizure frequency ($p = 0.294$), while significant within-group increases were observed in both groups ($p < 0.001$). Similarly, seizure duration (score ≥ 4) was significantly longer in the PTZ + ZAFIR group than in the PTZ group ($p < 0.001$). The temporal change in seizure duration was similar between the groups ($p = 0.450$), whereas significant within-group increases were observed in both groups ($p < 0.001$). Box plots of individual animal data for all behavioral seizure parameters are presented in Supplementary Fig. 5.

Open Field Maze Test

Animals in the SALINE group spent significantly more time in the center zone than those in the PTZ + ZAFIR group ($p = 0.018$). Representative heat maps illustrating the mean spatial distribution of each group are shown in Fig. 2C. No significant differences were observed among the groups in total distance traveled ($p = 0.170$), average speed ($p = 0.179$),

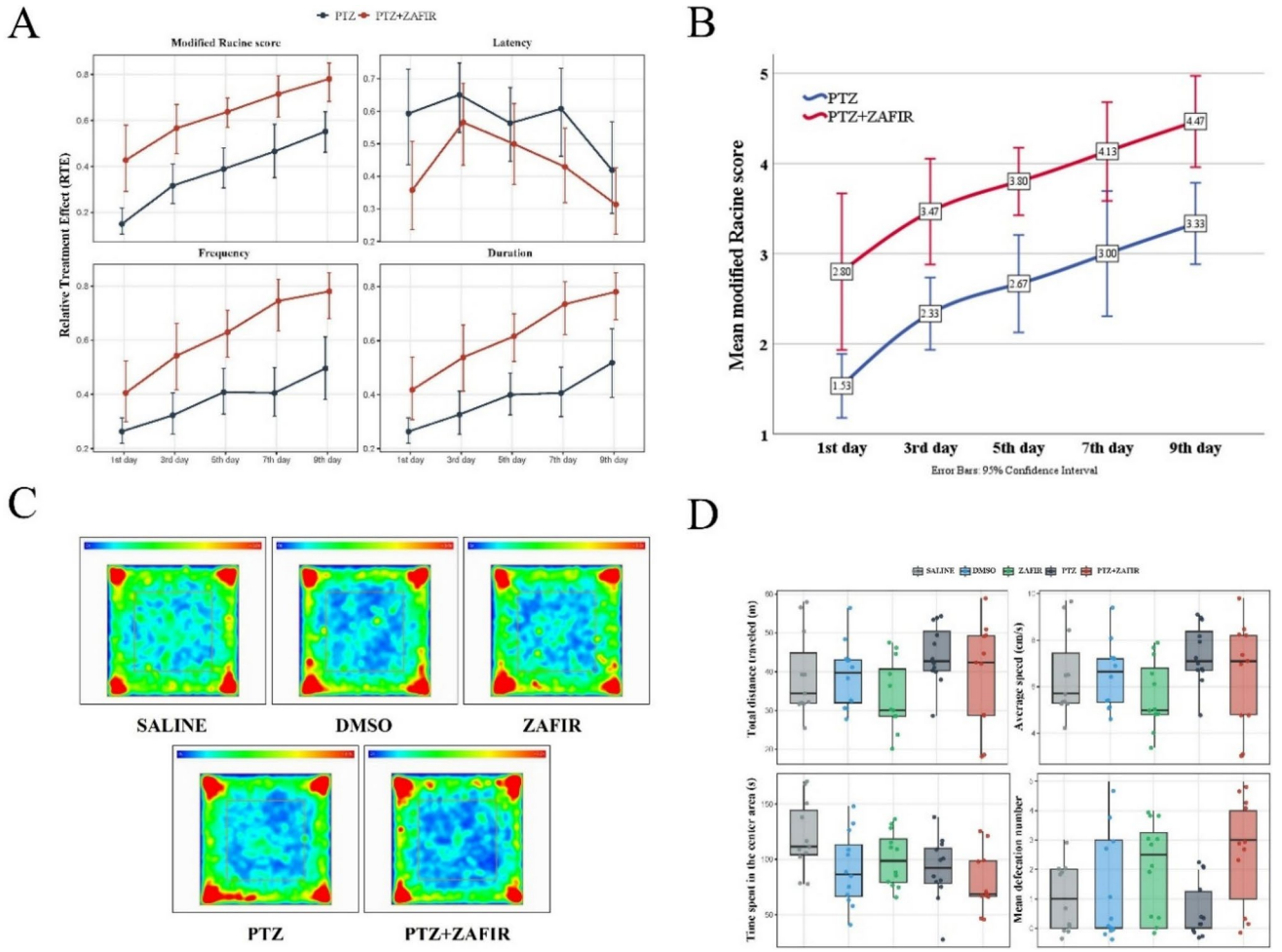

Fig. 2 **A** Graphics of relative treatment effects on seizure parameters with 95% confidence intervals. **B** Timeline graphics of seizure severity. PTZ + ZAFIR had more severe seizures than PTZ on all days $p < 0.001$. **C** Heatmaps of the groups in terms of mean time spent. While dark red represents 3 s, dark blue represents 0 s. **D** Box plots of individual animal data of open field maze

or fecal boli count (Bonferroni-corrected $p > 0.05$). Box plots of individual animal data from the open field test are presented in Fig. 2D. Detailed descriptive statistics, post hoc comparisons, and effect size estimates are provided in Supplementary Tables 1 and 2 (Supplementary File 2).

Blood Brain Barrier Permeability

Macroscopic evaluation revealed Evans Blue extravasation exclusively in the PTZ + ZAFIR group (Supplementary Fig. 6), and these findings were confirmed by microscopic analyses. Representative Evans Blue images are shown in Fig. 3. Fluorescence intensity was significantly higher in the PTZ + ZAFIR group than in all other groups in the DG ($p < 0.001$), CA1 ($p < 0.001$), CA3 ($p < 0.001$), and CC (vs. SALINE, $p = 0.005$; vs. DMSO, $p = 0.005$; vs. ZAFIR, $p = 0.004$; vs. PTZ, $p = 0.001$). In the CB, both the PTZ + ZAFIR group (vs. SALINE, $p = 0.015$; vs. DMSO, $p = 0.015$; vs. ZAFIR, $p = 0.018$) and the PTZ group (vs. SALINE, $p = 0.005$; vs. DMSO, $p = 0.004$; vs. ZAFIR, $p = 0.009$) exhibited significantly higher fluorescence intensity than the SALINE, DMSO, and ZAFIR groups, whereas no significant difference was observed between the PTZ and PTZ + ZAFIR groups. Across all regions except CA1, the PTZ group also exhibited significantly greater fluorescence intensity than the SALINE (DG and CA3, $p < 0.001$; CC, $p = 0.035$; CB, $p = 0.005$), DMSO (DG, $p < 0.001$; CA3, $p = 0.001$; CC, $p = 0.038$; CB, $p = 0.004$), and ZAFIR (DG, $p < 0.001$; CA3, $p = 0.001$; CC, $p = 0.036$; CB, $p = 0.009$) groups. In the CA1 region, the PTZ group exhibited higher mean fluorescence intensity than these groups; however, these differences were statistically significant. Detailed descriptive statistics, box plots of individual animal data, post hoc comparisons, and effect size estimates are provided in Supplementary File 3.

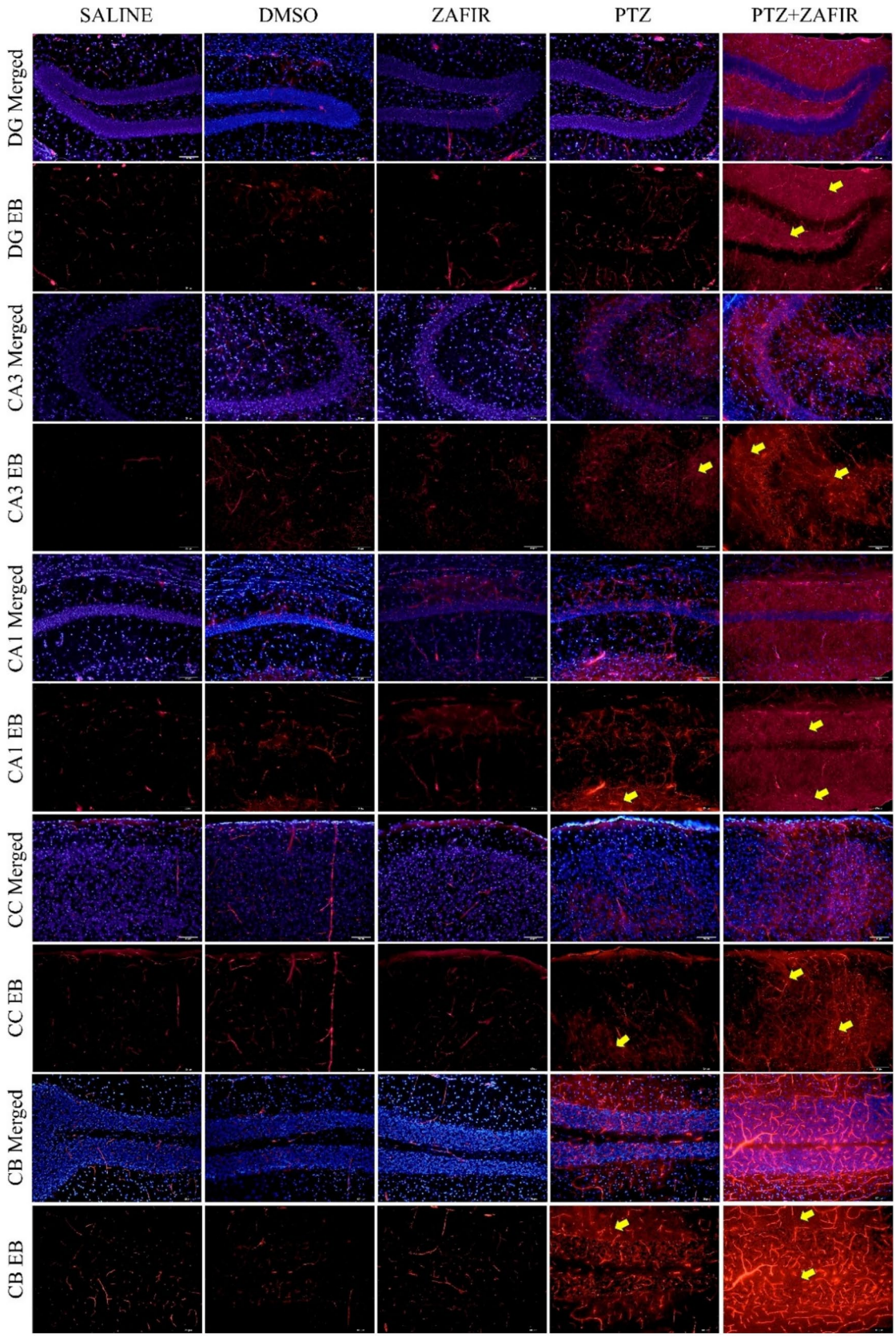

Fig. 3 Histological images of BBB permeability at 200× magnification. DG, dentate gyrus; CA, cornu ammonis; CC, cerebral cortex; CB, cerebellum; EB, Evans Blue. Blue color: DAPI. Red color: Evans Blue. Yellow arrows: extravasation of Evans Blue

Histological and Immunohistochemical Findings

Non-quantitative histopathological evaluation (Fig. 4) revealed minimal neuropil vacuolization and vascular congestion in the DMSO and ZAFIR groups. In the PTZ group, marked neuronal degeneration accompanied by pronounced pericellular and neuropil vacuolization was observed. In addition, severe vascular congestion was evident in the PTZ group. Compared with the PTZ group, the PTZ + ZAFIR group exhibited reduced neuronal degeneration, neuropil

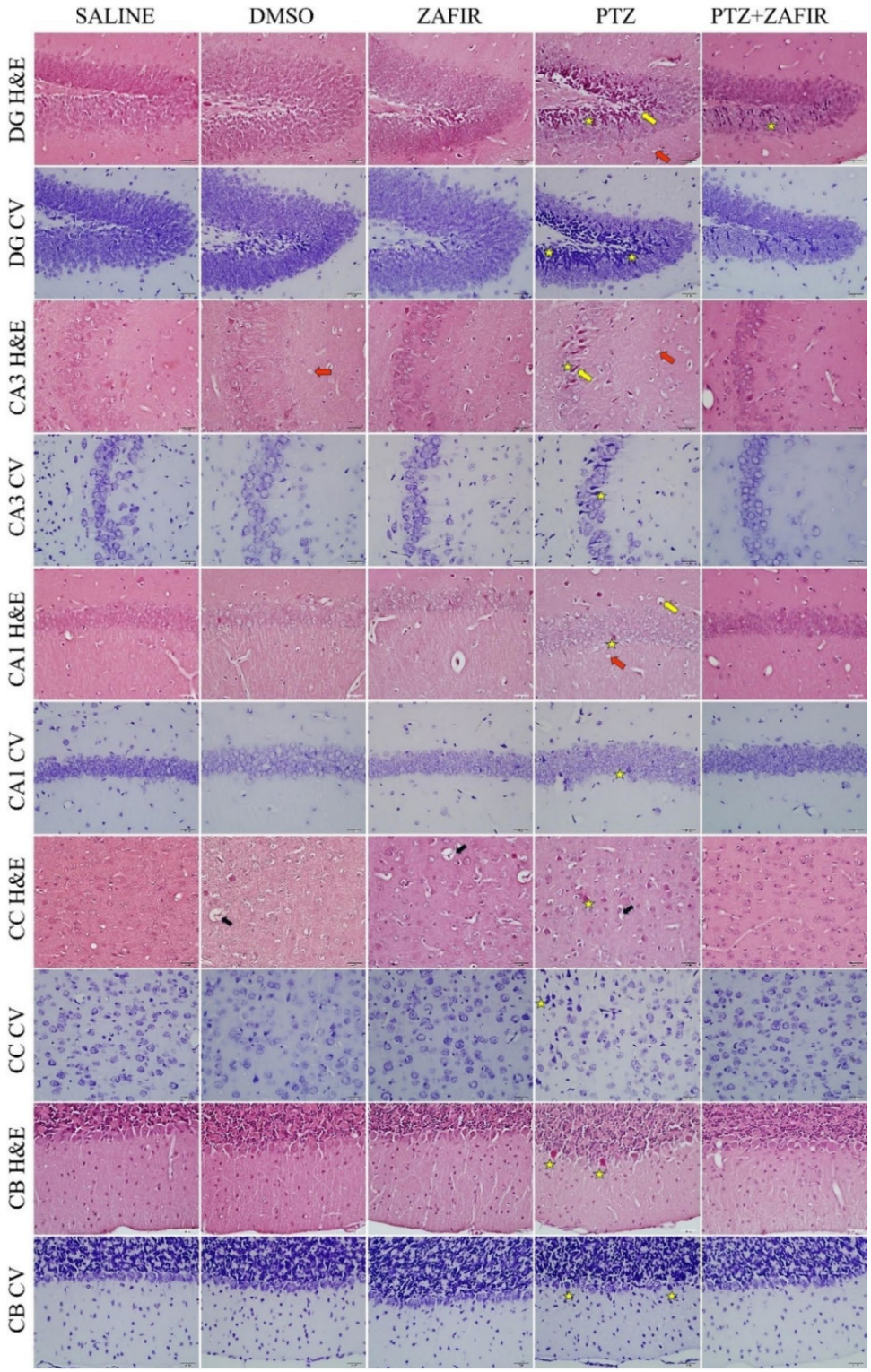

Fig. 4 Histological images of general tissue evaluation at 400× magnification. DG, dentate gyrus; CA, cornu ammonis; CC, cerebral cortex; CB, cerebellum; H&E, Hematoxylin and Eosin; CV, cresyl violet. Yellow stars: Degenerated neurons. Yellow arrows: Pericellular vacuolization. Red arrows: vacuolization in neuropil. Black arrows: congestive vessels

vacuolization, and vascular congestion. Among these histopathological findings, only the number of degenerated neurons was quantified and subjected to statistical analysis. Detailed descriptive statistics, box plots of individual animal data, post hoc comparisons, and effect size estimates are provided in Supplementary File 4. The PTZ group exhibited a significantly greater number of degenerated neurons than all other groups in every brain region examined (DG: vs. SALINE, DMSO, and ZAFIR, $p < 0.001$; vs. PTZ + ZAFIR, $p = 0.006$; CA1, CA3, and CC: vs. all other groups, $p = 0.020$; CB: vs. all other groups, $p < 0.001$).

Compared with the SALINE group, the PTZ + ZAFIR group showed a significantly higher number of degenerated neurons in the CC ($p = 0.020$). In the DG, the PTZ + ZAFIR group exhibited significantly more degenerated neurons than the SALINE, DMSO, and ZAFIR groups ($p = 0.001$). In the CA1 region, the ZAFIR group had significantly more degenerated neurons than the SALINE group ($p = 0.040$).

Anti-GFAP immunostaining (Fig. 5) showed predominantly resting astrocytes with thin, sparsely branched processes in the SALINE, DMSO, and ZAFIR groups. In the PTZ group, moderately reactive astrocytes were observed, with GFAP immunoreactivity predominantly localized around degenerated neurons. In contrast, the PTZ + ZAFIR group exhibited an increased number of reactive astrocytes with thick, highly branched processes. Detailed descriptive statistics, box plots of individual animal data, post hoc comparisons, and effect size estimates for anti-GFAP intensity are provided in Supplementary File 5. In the DG, the PTZ group exhibited significantly higher GFAP intensity than all other groups (vs. SALINE, DMSO, and ZAFIR, $p = 0.020$; vs. PTZ + ZAFIR, $p = 0.040$). The PTZ + ZAFIR group also showed significantly higher GFAP expressions than the SALINE, DMSO, and ZAFIR groups in the DG ($p = 0.020$). In the CA1, CA3, and CB regions, both the PTZ and PTZ + ZAFIR groups exhibited significantly higher GFAP expressions than the other groups ($p = 0.020$), with no significant difference between the two groups. In the CC, the PTZ + ZAFIR group exhibited significantly higher GFAP expressions than all other groups (vs. SALINE and DMSO, $p < 0.001$; vs. ZAFIR, $p = 0.003$; vs. PTZ, $p = 0.011$), whereas the PTZ group showed higher intensity than the SALINE and DMSO groups ($p < 0.001$). The ZAFIR group also exhibited higher GFAP expressions than the SALINE group in the CA1, CA3, and CB regions ($p = 0.020$).

Anti-Iba1 immunohistochemical images are shown in Fig. 6. Detailed descriptive statistics, box plots of individual animal data, post hoc comparisons, and effect size estimates for anti-Iba1 intensity are provided in Supplementary File 6. The PTZ group exhibited significantly higher Iba1 intensity than all other groups in the DG ($p = 0.020$), CA3 (vs. SALINE, $p = 0.004$; vs. DMSO, $p = 0.007$; vs. ZAFIR and PTZ + ZAFIR, $p = 0.006$), CA1 (vs. SALINE, $p = 0.007$; vs. DMSO, ZAFIR, and PTZ + ZAFIR, $p < 0.001$), and CC ($p < 0.001$). In the CB, the PTZ group also exhibited significantly higher

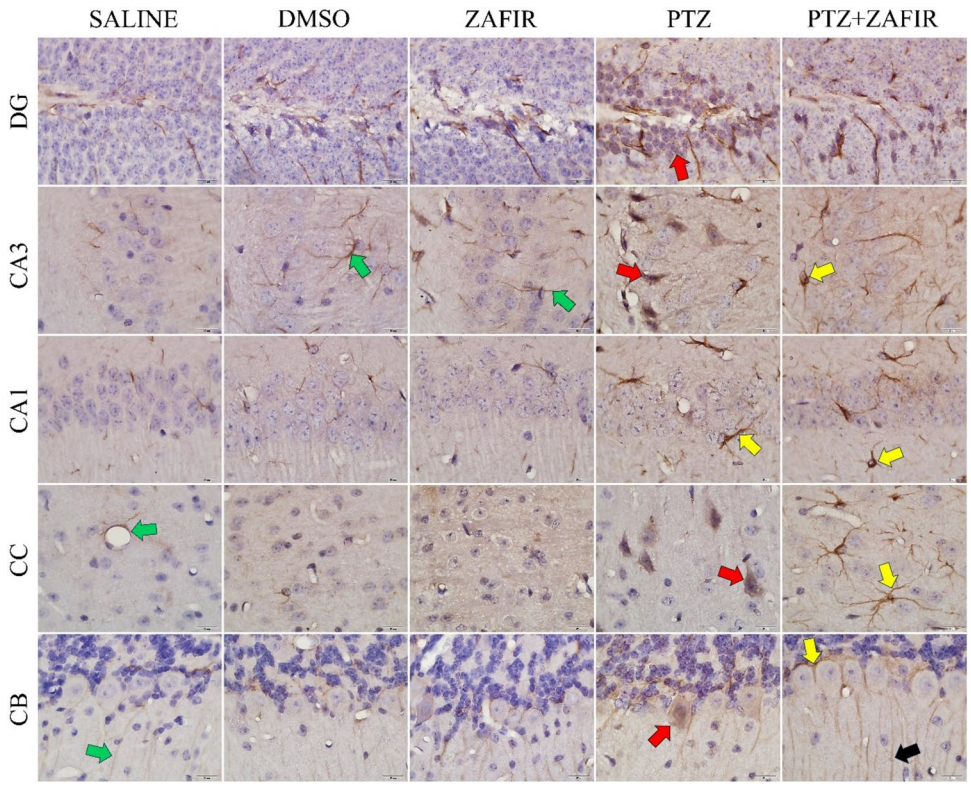

Fig. 5 Anti-GFAP immunostaining at 1000× magnification. DG, dentate gyrus. CA, cornu ammonis; CC, cerebral cortex; CB, cerebellum. Green arrows: resting astrocytes with thin processes. Red arrows: increased GFAP expression around degenerating neurons. Yellow arrows: active astrocytes with hypertrophied processes and increased branching. Black arrow: prominent Bergmann fibers

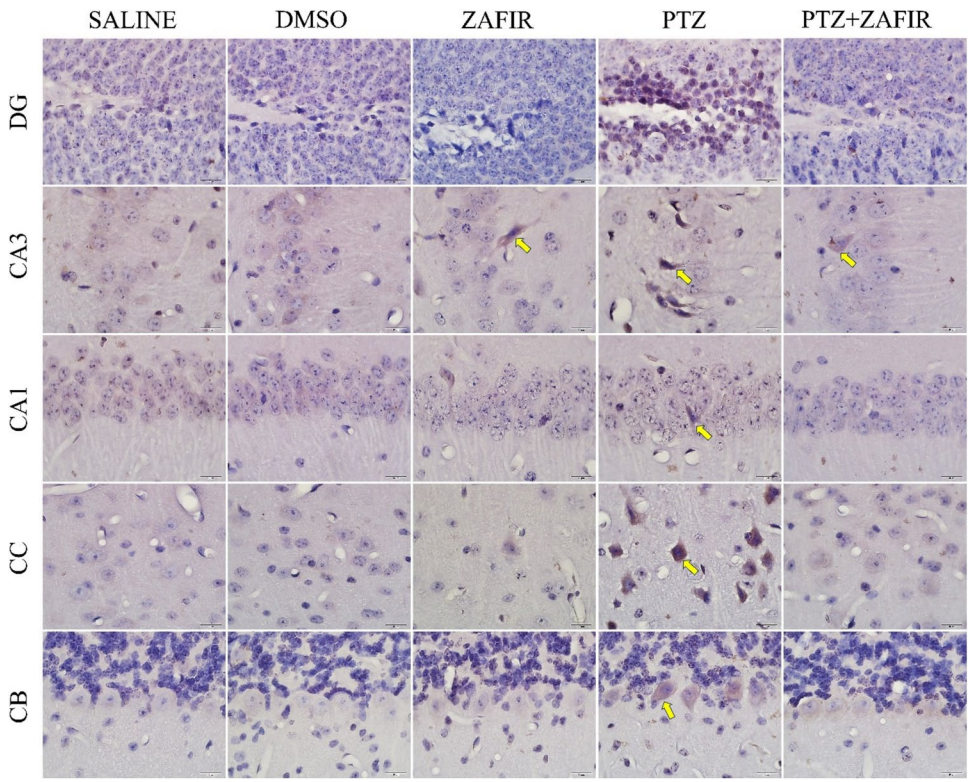

Fig. 6 Anti-Iba1 immunostaining at 1000× magnification. DG, dentate gyrus; CA, cornu ammonis; CC, cerebral cortex; CB, cerebellum. Yellow arrows: increased Iba1 expression around degenerating neurons

Iba1 intensity than the SALINE ($p = 0.002$) and DMSO ($p = 0.001$) groups. No significant differences were observed among the remaining groups.

Anti-NeuN immunohistochemical images are shown in Fig. 7. Detailed descriptive statistics, box plots of individual animal data, post hoc comparisons, and effect size estimates for anti-NeuN intensity are provided in Supplementary File 7. In the CA1 region, the SALINE, DMSO, and ZAFIR groups exhibited significantly higher NeuN intensity than both the PTZ and PTZ + ZAFIR groups ($p = 0.020$). In the CC, the DMSO group showed significantly higher NeuN intensity than the PTZ and PTZ + ZAFIR groups ($p < 0.001$). Similarly, the ZAFIR group exhibited higher intensity than the PTZ ($p < 0.001$) and PTZ + ZAFIR ($p = 0.002$) groups, while the SALINE group also showed higher intensity than the PTZ ($p = 0.002$) and PTZ + ZAFIR ($p = 0.009$) groups. In addition, the PTZ + ZAFIR group exhibited significantly higher NeuN intensity than the PTZ group ($p = 0.003$). In the DG, both the ZAFIR and DMSO groups exhibited significantly higher NeuN intensity than the PTZ and PTZ + ZAFIR groups (both $p < 0.001$). Furthermore, the ZAFIR group showed higher intensity than the SALINE group ($p = 0.002$), and the DMSO group showed higher intensity than the SALINE group ($p = 0.006$). The SALINE and PTZ groups also exhibited higher NeuN intensity than the PTZ + ZAFIR group ($p < 0.001$). In the CA3 region, the ZAFIR group exhibited significantly higher NeuN intensity than all other groups ($p < 0.001$). In addition, the DMSO group showed higher intensity than the PTZ ($p = 0.001$) and PTZ + ZAFIR ($p < 0.001$) groups, whereas the SALINE and PTZ groups exhibited higher intensity than the PTZ + ZAFIR group ($p < 0.001$). No significant differences were observed among the groups in the CB.

Anti-mouse serum albumin immunohistochemical images are shown in Fig. 8. Detailed descriptive statistics, box plots of individual animal data, post hoc comparisons, and effect size estimates for anti-mouse serum albumin intensity are provided in Supplementary File 8. The PTZ + ZAFIR group exhibited significantly higher anti-mouse serum albumin intensity than all other groups in the DG ($p < 0.001$), CC ($p = 0.020$), and CB ($p = 0.020$). In the CA3 and CA1 regions, the PTZ + ZAFIR group also showed significantly higher intensity than the SALINE, DMSO, and ZAFIR groups (both $p < 0.001$). PTZ had higher intensity than SALINE, DMSO and ZAFIR groups in the CA1 ($p < 0.001$), CC ($p = 0.020$), CB ($p = 0.020$). Also, PTZ had higher intensity than SALINE ($p = 0.002$), DMSO & ZAFIR ($p = 0.001$) in the CA3. The ZAFIR group exhibited significantly higher anti-mouse serum albumin intensity than SALINE and DMSO groups in the CC ($p = 0.020$).

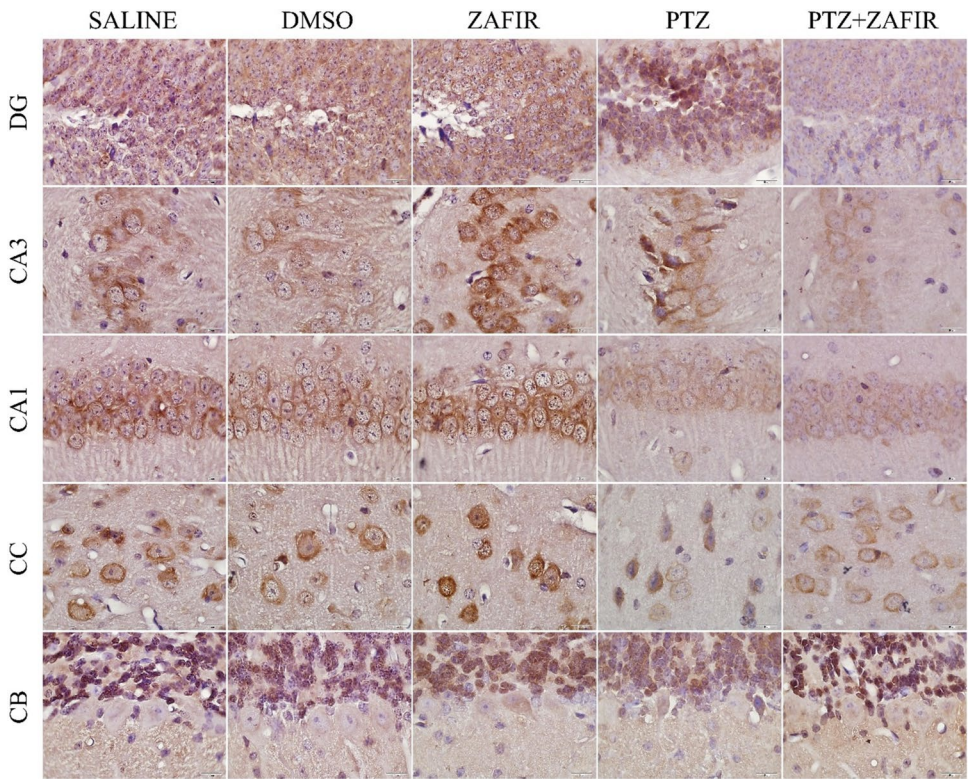

Fig. 7 Anti-NeuN immunostaining at 1000× magnification. DG, dentate gyrus; CA, cornu ammonis; CC, cerebral cortex; CB, cerebellum

Biochemical Analyses

Box plots of individual animal data for the ELISA measurements of IL-1β, MMP-9, and TGF-β1 are presented in Fig. 9. Detailed descriptive statistics, post hoc comparisons, and effect size estimates are provided in Supplementary File 9. Among these markers, a significant increase in cerebral TGF-β1 levels was observed in the PTZ + ZAFIR group compared with the SALINE group ($p = 0.020$). No significant differences were detected among the groups for IL-1β or MMP-9 levels. Box plots of individual animal data for the MDA and MPO analyses are presented in Fig. 10. Detailed descriptive statistics, post hoc comparisons, and effect size estimates are provided in Supplementary File 10. No significant differences were observed among the groups for either parameter.

Discussion

The role of BBB disruption and reactive gliosis in epileptogenesis has been well established. Following an initial brain insult, activation of astrocytes and microglia alters ion channel function, disrupts neuron–glia metabolic interactions, and promotes the release of pro-inflammatory mediators, thereby increasing neuronal excitability. This increased excitability predisposes the brain to recurrent seizures, which in turn induce further BBB damage and perpetuate a self-reinforcing pathological cycle [5]. The primary aim of the present study was to identify a therapeutic agent capable of interrupting this cascade during the early stages of epileptogenesis, before it becomes fully established. In an experimental model of ischemic brain injury in C57BL/6 mice, Zeng et al. demonstrated that zafirlukast reduced BBB permeability, increased the expression of the tight junction proteins ZO-1 and occludin, and suppressed MMP-2 and MMP-9 activity [14]. These findings prompted us to investigate zafirlukast as a potential therapeutic agent for preserving BBB integrity and consequently attenuating reactive gliosis and ultimately early epileptogenesis. Previous studies have reported that full kindling in PTZ-induced epileptogenesis models using C57BL/6 mice typically develops after approximately the tenth PTZ injection [15]. In the present study, the mean Modified Racine score in the PTZ group reached 3.4 ± 0.8 by the ninth day (5th PTZ injection), and only 27% of animals achieved full kindling, indicating that our experimental model progressed as expected and was consistent with previous reports. Unexpectedly, however, all behavioral seizure parameters were significantly exacerbated in the zafirlukast-treated animals (Supplementary File 1).

Previous studies investigating Cys-LTR antagonists under epileptic conditions have generally reported anticonvulsant and neuroprotective effects. Cevik et al. demonstrated that montelukast (50 and 100 mg/kg) reduced

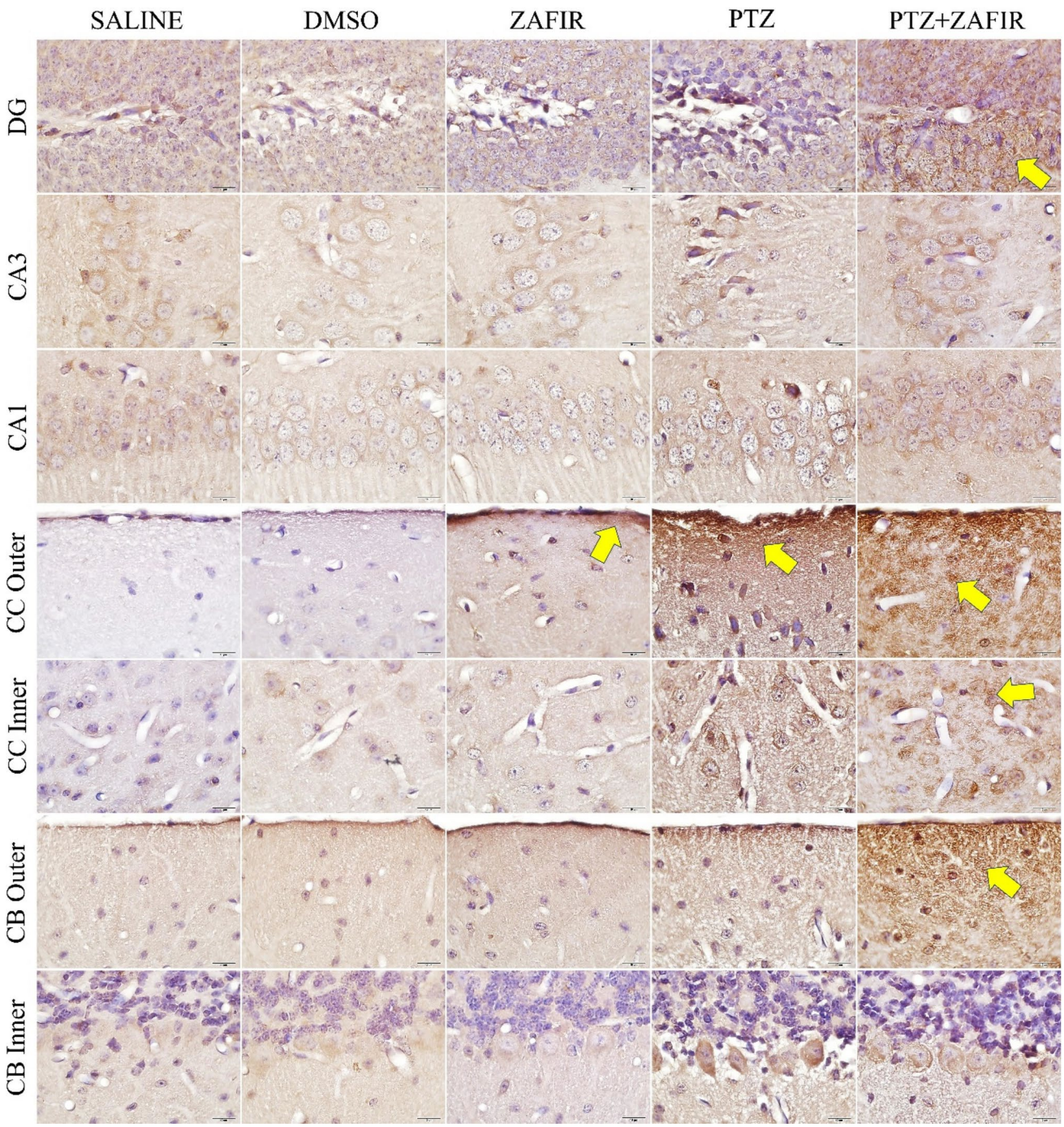

Fig. 8 Anti-mouse serum albumin immunostaining at 1000× magnification. DG, dentate gyrus; CA, cornu ammonis; CC, cerebral cortex; CB, cerebellum. Yellow arrows: albumin extravasation

EEG spike frequency following acute PTZ administration (35 mg/kg) in rats. Following PTZ administration at 70 mg/kg, the same doses also reduced Racine seizure scores and prolonged the latency to the first myoclonic jerk. Furthermore, montelukast treatment was associated with decreased MDA levels and increased SOD activity in brain tissue [13]. Fleck et al. reported that intracerebroventricular (i.c.v.) co-administration of montelukast with phenobarbital potentiated the anticonvulsant effect of phenobarbital in an acute PTZ model, whereas administration of LTD4 reversed this effect [10]. In another study by the same group, montelukast (10 mg/kg) increased the latency to generalized tonic–clonic seizures in PTZ-kindled animals [9]. Rehni et al. demonstrated dose-dependent suppression of both PTZ-induced

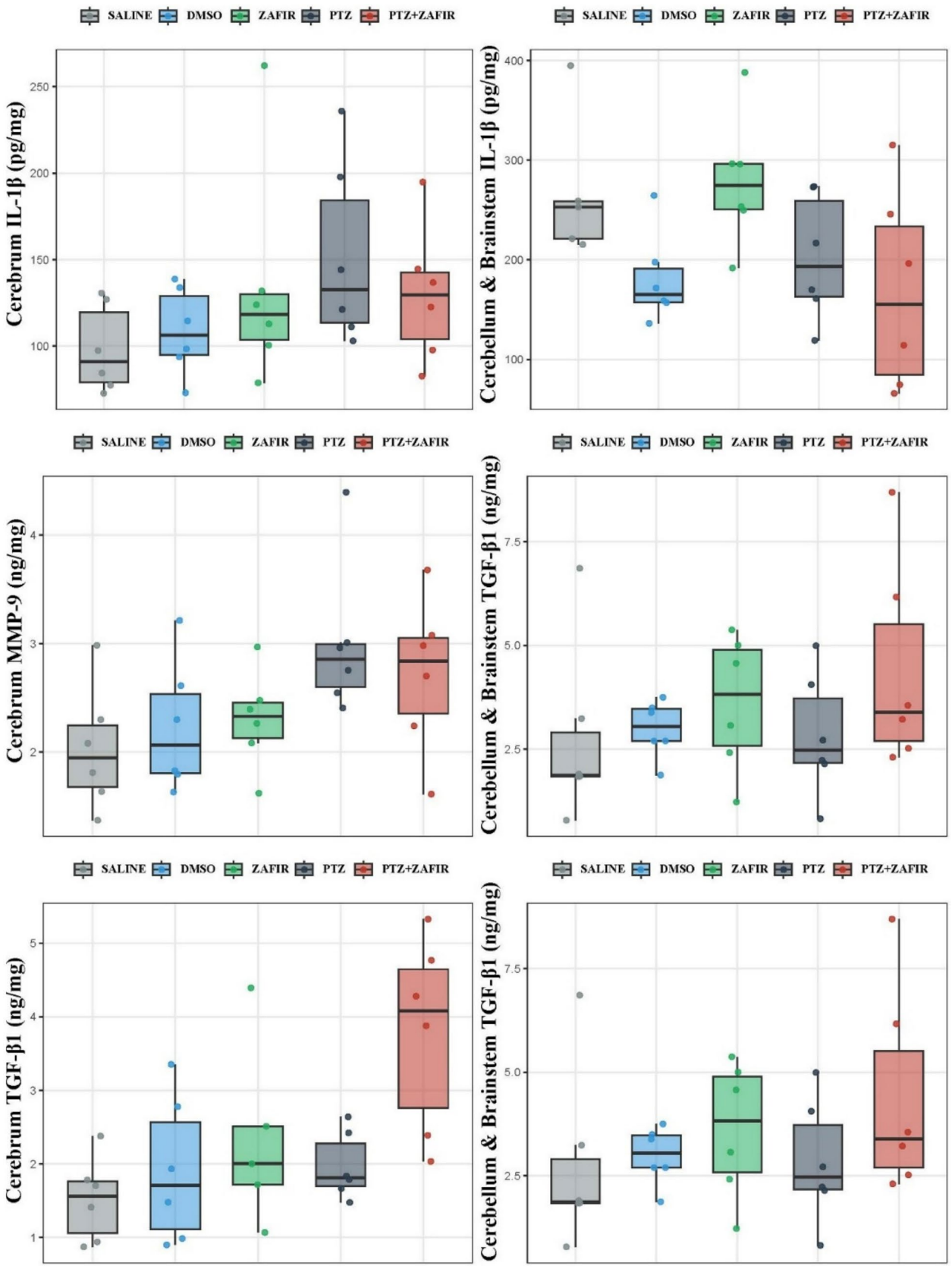

Fig. 9 Box plots of individual animal data for ELISA analyses

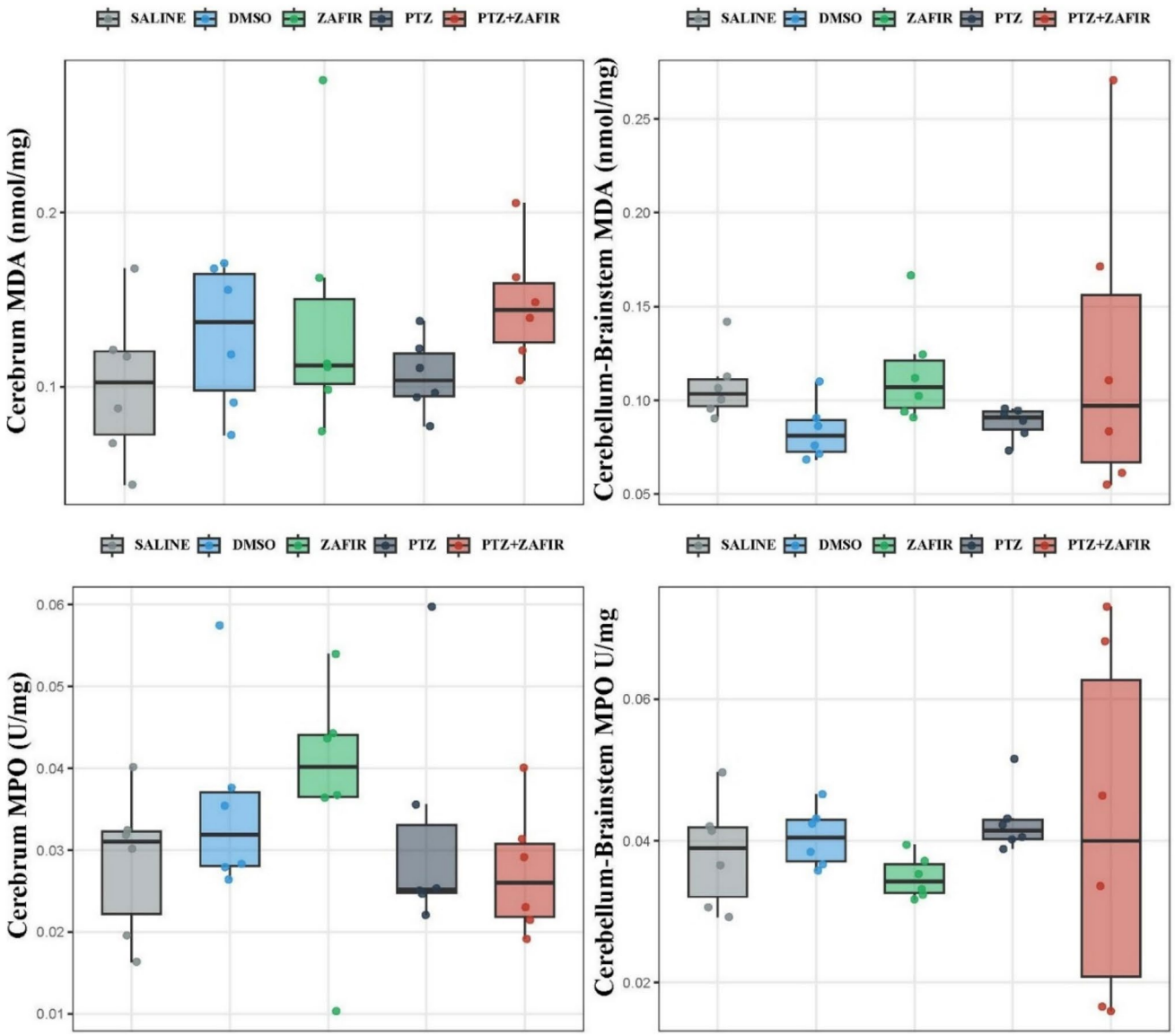

Fig. 10 Box plots of individual animal data for MDA-MPO analyses

kindling and spontaneous recurrent seizures following pilocarpine-induced status epilepticus after montelukast treatment (1, 3 and 10 mg/kg) [11]. Similarly, Lenz et al. showed that i.c.v. administration of montelukast and pranlukast prolonged seizure latency and reduced EEG amplitude following PTZ administration. In the same study, administration of i.c.v. LTD4 after montelukast reversed the anticonvulsant effect of montelukast. Montelukast reduced PTZ-induced BBB permeability and leukocyte migration, whereas LTD4 produced the opposite effects [12].

Several explanations may account for the discrepancy between our findings regarding behavioral seizure activity and the existing literature. First, unlike montelukast, zafirlukast has not previously been evaluated in experimental epilepsy models. Therefore, the beneficial effects reported for montelukast may not represent a class effect of all Cys-LTR antagonists. Second, although only mild histopathological alterations were observed, statistically significant adverse findings were detected exclusively in the ZAFIR group and not in the DMSO group. These observations may reflect previously unrecognized off-target effects of zafirlukast or an interaction between zafirlukast and its vehicle. For example, increased albumin extravasation in the CC of the ZAFIR group may itself represent an initiating event in epileptogenesis. Weissberg et al. demonstrated that i.c.v. administration of albumin enhances neuronal excitability through activation of the astrocytic TGF-β signaling pathway [24]. Consistent with this possibility, both the DMSO and ZAFIR groups exhibited mild neuropil vacuolization and vascular congestion compared with the SALINE group. Collectively, these

findings suggest that zafirlukast, at the dose and with the vehicle used in the present study, may have induced subtle histopathological alterations independently of PTZ administration. Such pre-existing tissue alterations may have increased susceptibility to subsequent PTZ-induced seizures. Alternatively, the dosing regimen or vehicle used in the present study may have shifted the balance between inhibitory and excitatory neurotransmission through mechanisms unrelated to Cys-LTR1 antagonism.

An important limitation of this study is that zafirlukast was evaluated using only a single dose and vehicle formulation. Previous studies investigating Cys-LTR antagonists employed a wide range of doses, administration routes (intracerebroventricular, intraperitoneal, and subcutaneous), vehicles (saline, immune serum, DMSO, and propylene glycol), and treatment schedules [9–13]. Therefore, differences in experimental design may partially explain the discrepant findings observed in the present study. Studies evaluating DMSO in PTZ-induced seizure models have generally reported that DMSO does not exacerbate PTZ-induced seizure activity [25–27]. Furthermore, according to the Washington State University Institutional Animal Care and Use Committee guidelines, DMSO concentrations used as vehicles in vivo studies should not exceed 10% (v/v), with a maximum dose of 2 mL/kg [28]. In another study, repeated administration of DMSO (10 mL/kg/day for 10 days) at concentrations of 1.8%, 3.6%, and 7.2% produced no motor deficits, although transient mechanical allodynia occurred at the two higher concentrations [29]. Therefore, based on the available literature, the DMSO concentration and dose used in the present study would not be expected to potentiate PTZ-induced seizures directly. Nevertheless, the qualitative histopathological changes observed in the DMSO group raise the possibility that repeated DMSO administration may have produced cumulative tissue effects.

Another possible explanation involves a pharmacokinetic interaction between zafirlukast and PTZ. To minimize direct interaction, zafirlukast was administered twice daily, whereas PTZ was administered at midday. Nevertheless, zafirlukast is known to inhibit the hepatic CYP2C9 and CYP3A isoenzymes in vitro, reduce warfarin clearance, and increase its plasma concentration in healthy volunteers [30]. Because PTZ is primarily eliminated through hepatic metabolism [31], inhibition of hepatic drug metabolism by zafirlukast may have increased PTZ exposure and thereby potentiated its proconvulsant effects. In addition, strain- and sex-dependent factors should also be considered. Previous studies evaluating Cys-LTR antagonists in epilepsy conditions used Sprague–Dawley rats, Swiss mice, or Swiss albino mice [9–13], whereas the present study was conducted in C57BL/6 mice. Therefore, strain-specific differences may have contributed to the observed discrepancies. As another limitation of our study, only male mice were included in the present study, precluding assessment of sex-dependent effects. Taken together, our findings suggest that the effects of zafirlukast on early epileptogenesis may depend on the dose, vehicle formulation, administration schedule, animal strain, sex, and experimental model. Future studies employing different dosing regimens, vehicle formulations, animal strains, and both sexes will be necessary to clarify the role of zafirlukast in early epileptogenesis and its impact on behavioral seizure outcomes.

Anxiety is a common comorbidity in patients with epilepsy [1], and PTZ is known to induce anxiety-like behavior in experimental epilepsy models [32, 33]. In the present study, the PTZ + ZAFIR group exhibited more anxiety-like behavior in the open field maze than the SALINE group. Notably, this group experienced the most severe seizures and received the greatest number of injections throughout the experimental period. Therefore, the increased anxiety observed in this group may not be attributable solely to the effects of zafirlukast. Consistent with this interpretation, repeated injections have been reported to increase glucocorticoid levels in experimental animals [34]. The PTZ + ZAFIR group was also the only group in which Evans Blue extravasation was detectable macroscopically, and it exhibited the greatest BBB permeability in the microscopic analyses based on Evans Blue and anti-mouse serum albumin immunostaining. Given that this group experienced the most severe seizures, the greater degree of BBB disruption was not unexpected. However, the absence of a corresponding increase in MMP-9 levels suggests that BBB disruption may have been driven primarily by seizure-related mechanical stress rather than by robust inflammatory responses or reactive gliosis [35]. Surprisingly, despite increased GFAP immunoreactivity in the PTZ + ZAFIR group, we observed reduced Iba1 immunoreactivity and fewer degenerated neurons compared with the PTZ group. In addition, TGF-β1, a key astrocyte-associated cytokine involved in reactive gliosis [36], was significantly increased in the cerebrum of the PTZ + ZAFIR group compared with the SALINE group. In contrast, MMP-9 and IL-1β levels did not increase despite the greater seizure severity observed in the PTZ + ZAFIR group (35,37,38). Likewise, MDA and MPO levels remained unchanged [39]. These findings suggest that zafirlukast may differentially modulate astrocytic and microglial responses during early epileptogenesis. While increased GFAP immunoreactivity and TGF-β1 levels are consistent with enhanced astrocyte activation, the reductions in Iba1 immunoreactivity and neuronal degeneration may indicate suppression of microglial activation and its associated neurotoxic effects.

Previous studies have demonstrated that modulation of oxidative stress-related pathways can influence seizure susceptibility and disease progression in experimental epilepsy models [40, 41]. NADPH oxidase (NOX), particularly NOX2, has been identified as an important source of

reactive oxygen species (ROS) generation during epileptic conditions, and pharmacological or genetic inhibition of NOX2 has been associated with reduced seizure severity and improved neurological outcomes [42–45]. Similarly, activation of the transcription factor Nrf2, which plays a protective role against oxidative stress, has been shown to attenuate seizure severity [46, 47]. In addition to oxidative stress, emerging evidence indicates that pyroptosis-related inflammatory cell death pathways may contribute to neuronal injury and epileptogenesis [48, 49]. Pharmacological activation of AMP-activated protein kinase (AMPK) has been reported to suppress pyroptotic responses [50], whereas inhibition of absent in melanoma 2 (AIM2)-associated inflammasome signaling has been linked to reduced neuronal damage and improved outcomes in experimental models [51, 52]. The potential neuroprotective effects of zafirlukast observed in the present study may therefore involve modulation of oxidative stress and pyroptosis-related pathways. Considering the reduction in neuronal degeneration and microglial activation observed in the PTZ + ZAFIR group despite increased behavioral seizure severity, it is possible that zafirlukast may influence downstream pathways associated with oxidative stress, inflammatory cell death, or neuronal survival. However, these mechanisms remain speculative, as oxidative stress markers, pyroptosis-related proteins, and antioxidant pathway components were not directly evaluated in the present study. Furthermore, the absence of significant differences in MDA and MPO levels should be interpreted cautiously. Since biochemical analyses were performed using relatively broad brain tissue homogenates, region-specific alterations occurring in areas such as the hippocampus or cortex may have been diluted and therefore not detectable.

When all the findings are evaluated together, our results suggest that zafirlukast may exert paradoxical effects during PTZ-induced early epileptogenesis. On the one hand, zafirlukast may promote astrocyte activation through albumin extravasation–induced activation of the TGF-β1 signaling pathway. On the other hand, the reduced Iba1 immunoreactivity in the PTZ + ZAFIR group, together with the absence of the expected increase in IL-1β, a key pro-inflammatory cytokine predominantly released by activated microglia [53], despite the greater seizure severity, suggests that microglia-mediated inflammatory pathways may have been suppressed. Previous studies have shown that inhibition of microglial activation can reduce neurodegeneration. In mice, administration of macrophage/microglia inhibitory factor markedly reduced kainic acid-induced neurodegeneration [54]. Likewise, in a mouse model of amyotrophic lateral sclerosis, inhibition of the microglial NF-κB pathway reduced motor neuron death, whereas activation of the same pathway exacerbated neuronal loss. In contrast, inhibition of NF-κB signaling in astrocytes did not affect neuronal survival [55]. These findings support the possibility that the reduced neuronal degeneration observed in the PTZ + ZAFIR group may be related, at least in part, to suppression of microglial activation. In the present study, the potential neuroprotective effects of zafirlukast may therefore involve modulation of oxidative stress- and neuronal death–related pathways, as well as attenuation of microglia-mediated inflammatory responses. The absence of significant increases in IL-1β and other inflammatory markers in the PTZ group may reflect the relatively early stage of epileptogenesis, as only 27% of the animals had reached full kindling by the end of the experimental period.

Limitations of the Study

Several limitations of the present study should be acknowledged. First, zafirlukast was evaluated using only a single dose (10 mg/kg administered i.p. twice daily), a single vehicle formulation (1% DMSO), and a fixed administration schedule. Therefore, the dose dependency of the observed effects and the potential influence of alternative vehicle formulations or dosing regimens could not be assessed. In addition, although the DMSO concentration used in the present study was within recommended limits and previous studies have not reported exacerbation of PTZ-induced seizures with DMSO alone, the mild qualitative histopathological changes observed in the DMSO group raise the possibility of cumulative effects following repeated administration. Consequently, a pharmacological interaction between zafirlukast, DMSO, and PTZ cannot be completely excluded. Second, only a single experimental model of epilepsy was used. Since previous studies investigating Cys-LTR antagonists have employed different epilepsy models, animal strains, routes of drug administration, and experimental protocols, the generalizability of the present findings remains uncertain. Third, only male C57BL/6 mice were included in the study. Therefore, potential sex-dependent and strain-dependent differences in the effects of zafirlukast could not be evaluated. Fourth, biochemical analyses were performed using whole-tissue homogenates rather than region-specific brain samples. Consequently, localized molecular changes within individual brain regions may have been diluted, potentially masking biologically relevant differences in inflammatory and oxidative stress markers. In addition to this, the present study focused primarily on behavioral, histopathological, and biochemical outcomes. Although our findings suggest that zafirlukast may differentially modulate astrocytic and microglial responses, the underlying molecular mechanisms, including the involvement of NF-κB, oxidative stress, pyroptosis, and cytokine-related signaling pathways, were not directly investigated. Furthermore, the possibility that zafirlukast altered PTZ pharmacokinetics through inhibition of hepatic drug-metabolizing enzymes could not be examined. Despite these limitations, this study provides the first comprehensive evaluation of zafirlukast in a PTZ-induced model of early epileptogenesis, integrating

behavioral, blood–brain barrier, histopathological, and biochemical assessments. The findings identify previously unrecognized paradoxical effects of zafirlukast and provide a foundation for future mechanistic studies.

Future Directions

The unexpected findings of the present study warrant further investigation into the role of zafirlukast during early epileptogenesis. Future studies should first determine whether the observed effects are dose-, vehicle-, or administration schedule-dependent by evaluating multiple dosing regimens, alternative vehicle formulations, and different treatment paradigms. Because zafirlukast may also influence PTZ pharmacokinetics through inhibition of hepatic CYP enzymes, pharmacokinetic studies are needed to determine whether altered PTZ metabolism contributes to the exacerbation of seizure activity. Validation of the present findings in different experimental epilepsy models, including chemoconvulsant and post-traumatic epileptogenesis models, as well as in different animal strains and both sexes, will be essential to establish the reproducibility and generalizability of these observations. Region-specific biochemical and molecular analyses should also be performed to avoid dilution effects associated with whole-brain homogenates and to better characterize localized inflammatory and neurodegenerative responses. Mechanistic studies are required to clarify how zafirlukast differentially regulates astrocytic and microglial responses during epileptogenesis. Future investigations should examine the involvement of TGF-β, NF-κB, IL-1β, oxidative stress, pyroptosis, and other cell death–related signaling pathways using complementary molecular approaches. Additional evaluation of blood–brain barrier integrity by assessing tight junction proteins, including occludin, claudin-5, and ZO-1, together with matrix metalloproteinase activity, may further elucidate the mechanisms underlying the increased BBB permeability observed in the present study. Finally, combining behavioral assessments with electrophysiological recordings and advanced molecular profiling may provide a more comprehensive understanding of the paradoxical effects of zafirlukast during epileptogenesis and help determine whether these findings represent a drug-specific effect or reflect previously unrecognized complexity in cysteinyl leukotriene receptor signaling.

Conclusion

Zafirlukast, administered at 10 mg/kg twice daily in 1% DMSO, significantly exacerbated behavioral seizure activity in the PTZ-induced model of early epileptogenesis. Our findings suggest that zafirlukast exerts paradoxical effects on reactive gliosis. While it may promote astrocyte activation, potentially through albumin extravasation and activation of the TGF-β signaling pathway, it was also associated with reduced microglial activation and decreased neuronal degeneration. These opposing effects suggest that zafirlukast may differentially modulate astrocytic and microglial responses during early epileptogenesis, potentially involving NF-κB- and IL-1β-related signaling pathways. Additional mechanisms may include modulation of oxidative stress and neuronal death pathways.

The increased behavioral seizure activity observed in the present study cannot be attributed solely to alterations in BBB permeability or reactive gliosis, as epileptogenesis is a multifactorial process involving neuronal network excitability and immune-mediated mechanisms. The contribution of these pathways to the effects of zafirlukast requires further investigation. Future studies incorporating electrophysiological assessments, region-specific molecular analyses, and immune profiling will be important to clarify the mechanisms underlying the effects of zafirlukast during early epileptogenesis.

Supplementary Information The online version contains supplementary material available at https://doi.org/10.1007/s12035-026-06110-5.

Acknowledgements We thank Ege University Research and Application Center of Drug Development and Pharmacokinetics (ARGEFAR) for collaboration. We are grateful to Stoelting Europe (Dublin, Ireland) and Cinzia Boldi for free trial of ANY-maze 7.2 software. We thank Levent Muslular for production of plexiglass cages. This publication is derived from Volkan GÖRGÜLÜ's PhD thesis of specialization in medicine.

Author Contributions Conception and design of the study: VG, AY, NUKY, EYS and TK, Animal Experiments: VG, AY, ES. Histological Analyses: VG, CST, AB, BO, AY. Biochemical Analyses: PE, EYS, VG. Statistical Analyses: TK, VG. Manuscript draft: All authors.

Funding This study was funded by Ege University Scientific Research Projects (TTU-2021-22874).

Data Availability No datasets were generated or analyzed during the current study.

Declarations

Ethics Approval The experimental protocol was evaluated and approved by Ege University, Local Ethics Committee for Animal Experiments (Approval No: 2020-119).

Conflict of interest The authors declare that there is no conflict of interest.

References

1. World Health Organization (2019) Epilepsy: a public health imperative. World Health Organization. https://iris.who.int/handle/10665/325293
2. Brodie MJ, Barry SJ, Bamagous GA, Norrie JD, Kwan P (2012) Patterns of treatment response in newly diagnosed epilepsy. Neurology 78:1548–1554. https://doi.org/10.1212/WNL.0b013e3182563b19
3. Thurman DJ, Begley CE, Carpio A, Helmers S, Hesdorffer DC, Mu J et al (2018) The primary prevention of epilepsy: a report of

the Prevention Task Force of the International League Against Epilepsy. Epilepsia 59:905–914. https://doi.org/10.1111/epi.14068
4. Pitkänen A, Lukasiuk K, Dudek FE, Staley KJ (2015) Epileptogenesis. Cold Spring Harb Perspect Med 5. https://doi.org/10.1101/cshperspect.a022822
5. Patel DC, Tewari BP, Chaunsali L, Sontheimer H (2019) Neuron-glia interactions in the pathophysiology of epilepsy. Nat Rev Neurosci 20:282–297. https://doi.org/10.1038/s41583-019-0126-4
6. Shao LR, Habela CW, Stafstrom CE (2019) Pediatric epilepsy mechanisms: expanding the paradigm of excitation/inhibition imbalance. Children (Basel) 6:23. https://doi.org/10.3390/children6020023
7. Rana A, Musto AE (2018) The role of inflammation in the development of epilepsy. J Neuroinflammation 15:144. https://doi.org/10.1186/s12974-018-1192-7
8. Ghosh A, Chen F, Thakur A, Hong H (2016) Cysteinyl leukotrienes and their receptors: emerging therapeutic targets in central nervous system disorders. CNS Neurosci Ther 22:943–951. https://doi.org/10.1111/cns.12596
9. Fleck J, Temp FR, Marafiga JR, Jesse AC, Milanesi LH, Rambo LM et al (2016) Montelukast reduces seizures in pentylenetetrazol-kindled mice. Braz J Med Biol Res 49. https://doi.org/10.1590/1414-431X20155031
10. Fleck J, Marafiga JR, Jesse AC, Ribeiro LR, Rambo LM, Mello CF (2015) Montelukast potentiates the anticonvulsant effect of phenobarbital in mice: an isobolographic analysis. Pharmacol Res 94:34–41. https://doi.org/10.1016/j.phrs.2015.02.001
11. Rehni AK, Singh TG (2011) Modulation of leukotriene D4 attenuates the development of seizures in mice. Prostaglandins Leukot Essent Fatty Acids 85:97–106. https://doi.org/10.1016/j.plefa.2011.04.003
12. Lenz QF, Arroyo DS, Temp FR, Poersch AB, Masson CJ, Jesse AC et al (2014) Cysteinyl leukotriene receptor (CysLT) antagonists decrease pentylenetetrazol-induced seizures and blood-brain barrier dysfunction. Neuroscience 277:859–871. https://doi.org/10.1016/j.neuroscience.2014.07.058
13. Cevik B, Solmaz V, Aksoy D, Erbas O (2015) Montelukast inhibits pentylenetetrazol-induced seizures in rats. Med Sci Monit 21:869–874. https://doi.org/10.12659/MSM.892932
14. Shimada T, Yamagata K (2018) Pentylenetetrazole-induced kindling mouse model. J Vis Exp 136:56573. https://doi.org/10.3791/56573
15. Zeng C, Wang D, Chen C, Chen L, Chen B, Li L et al (2020) Zafirlukast protects blood-brain barrier integrity from ischemic brain injury. Chem Biol Interact 316. https://doi.org/10.1016/j.cbi.2019.108915
16. Racine RJ (1972) Modification of seizure activity by electrical stimulation: II. Motor seizure. Electroencephalogr Clin Neurophysiol 32:281–294. https://doi.org/10.1016/0013-4694(72)90177-0
17. Zhang YF, Li SL, Xiong TQ, Yang LB, Li YN, Tan BH et al (2014) The rearrangement of filamentous actin in mossy fiber synapses in pentylenetetrazol-kindled C57BL/6 mice. Epilepsy Res 108:20–28. https://doi.org/10.1016/j.eplepsyres.2013.10.019
18. Zou Y, Wang C, Li H, Zhong M, Lin J, Hu Y et al (2024) Epileptic seizures induced by pentylenetetrazole kindling accelerate Alzheimer-like neuropathology in 5×FAD mice. Front Pharmacol 15. https://doi.org/10.3389/fphar.2024.1500105
19. Seibenhener ML, Wooten MC (2015) Use of the open field maze to measure locomotor and anxiety-like behavior in mice. J Vis Exp 96:52434. https://doi.org/10.3791/52434
20. Gould TD, Dao DT, Kovacsics CE (2009) Mood and anxiety related phenotypes in mice. NeuroMethods 42:1–20. https://doi.org/10.1007/978-1-60761-303-9
21. Ueno H, Takahashi Y, Suemitsu S, Murakami S, Kitamura N, Wani K et al (2020) Effects of repetitive gentle handling of male C57BL/6NCrl mice on comparative behavioural test results. Sci Rep 10. https://doi.org/10.1038/s41598-020-60530-4
22. Petronilho F, Goldman JL, Barichello T (2019) Evans blue-albumin as a marker to evaluate blood-brain barrier integrity in neonatal and adult rodents. NeuroMethods 142:197–203. https://doi.org/10.1007/978-1-4939-8946-1_12
23. Lowry OH, Rosebrough NJ, Farr AL, Randall RJ (1951) Protein measurement with the Folin phenol reagent. J Biol Chem 193:265–275. https://doi.org/10.1016/s0021-9258(19)52451-6
24. Weissberg I, Wood L, Kamintsky L, Vazquez O, Milikovsky DZ, Alexander A et al (2015) Albumin induces excitatory synaptogenesis through astrocytic TGF-β/ALK5 signaling in a model of acquired epilepsy following blood–brain barrier dysfunction. Neurobiol Dis 78:115–125. https://doi.org/10.1016/j.nbd.2015.02.029
25. Fang Q, Zheng S, Chen Q, Chen L, Yang Y, Wang Y et al (2023) The protective effect of inhibiting mitochondrial fission on the juvenile rat brain following PTZ kindling through inhibiting the BCL2L13/LC3 mitophagy pathway. Metab Brain Dis 38:453–466. https://doi.org/10.1007/s11011-022-01077-3
26. Asadi-Shekaari M, Eslami A, Kalantaripour T, Joukar S (2014) Potential mechanisms involved in the anticonvulsant effect of walnut extract on pentylenetetrazole-induced seizure. Med Princ Pract 23:538–543. https://doi.org/10.1159/000365759
27. Jie L, Guohui J, Chen Y, Chen L, Li Z, Wang Z et al (2014) Altered expression of hypoxia-inducible factor-1α participates in the epileptogenesis in animal models. Synapse 68:402–409. https://doi.org/10.1002/syn.21752
28. Washington State University Institutional Animal Care and Use Committee (2022) Preparation of Dimethyl Sulfoxide; Standard Operating Procedures for Preparation of Dimethyl Sulfoxide. https://iacuc.wsu.edu/documents/2016/06/wsu_sop_1.pdf. Accessed 23 Jan 2026
29. Authier N, Dupuis E, Kwasiborski A, Eschalier A, Coudoré F (2002) Behavioural assessment of dimethylsulfoxide neurotoxicity in rats. Toxicol Lett 132:117–121. https://doi.org/10.1016/S0378-4274(02)00052-8
30. Dekhuijzen PN, Koopmans PP (2002) Pharmacokinetic profile of zafirlukast. Clin Pharmacokinet 41:105–114. https://doi.org/10.2165/00003088-200241020-00003
31. Jun HW (1976) Pharmacokinetic studies of pentylenetetrazol in dogs. J Pharm Sci 65:1038–1041. https://doi.org/10.1002/jps.2600650720
32. Anesti M, Stavropoulou N, Atsopardi K, Lamari FN, Panagopoulos NT, Margarity M (2020) Effect of rutin on anxiety-like behavior and activity of acetylcholinesterase isoforms in specific brain regions of pentylenetetrazol-treated mice. Epilepsy Behav 102. https://doi.org/10.1016/j.yebeh.2019.106632
33. Kordi Jaz E, Moghimi A, Fereidoni M, Asadi S, Shamsizadeh A, Roohbakhsh A (2017) SB-334867, an orexin receptor 1 antagonist, decreased seizure and anxiety in pentylenetetrazol-kindled rats. Fundam Clin Pharmacol 31:201–207. https://doi.org/10.1111/fcp.12249
34. Drude S, Geißler A, Olfe J, Starke A, Domanska G, Schuett C et al (2011) Side effects of control treatment can conceal experimental data when studying stress responses to injection and psychological stress in mice. Lab Anim 40:119–128. https://doi.org/10.1038/laban0411-119
35. Mizoguchi H, Yamada K (2013) Roles of matrix metalloproteinases and their targets in epileptogenesis and seizures. Clin Psychopharmacol Neurosci 11:45–52. https://doi.org/10.9758/cpn.2013.11.2.45
36. Cacheaux LP, Ivens S, David Y, Lakhter AJ, Bar-Klein G, Shapira M et al (2009) Transcriptome profiling reveals TGF-β signaling

involvement in epileptogenesis. J Neurosci 29:8927–8935. https://doi.org/10.1523/JNEUROSCI.0430-09.2009
37. Li G, Bauer S, Nowak M, Norwood B, Tackenberg B, Rosenow F et al (2011) Cytokines and epilepsy. Seizure 20:249–256. https://doi.org/10.1016/j.seizure.2010.12.005
38. Nieoczym D, Socała K, Zelek-Molik A, Pieróg M, Przejczowska-Pomierny K, Szafarz M et al (2021) Anticonvulsant effect of pterostilbene and its influence on the anxiety- and depression-like behavior in the pentetrazol-kindled mice: behavioral, biochemical, and molecular studies. Psychopharmacology 238:3167–3181. https://doi.org/10.1007/s00213-021-05933-5
39. El-Sayed RM, Fawzy MN, Zaki HF, Abd El-Haleim EA (2023) Neuroprotection impact of biochanin A against pentylenetetrazol-kindled mice: targeting NLRP3 inflammasome/TXNIP pathway and autophagy modulation. Int Immunopharmacol 115. https://doi.org/10.1016/j.intimp.2023.109711
40. Singh PK, Maurya S, Saadi A, Sandouka S, Zhang T, Kadosh O et al (2026) Thioredoxin-mimetic peptide attenuates epilepsy progression and neurocognitive deficits. Redox Biol 90. https://doi.org/10.1016/j.redox.2026.104021
41. Singh PK, Lignani G, Walker MC, Lieb A, Shekh-Ahmad T (2026) Activity-dependent antioxidant gene therapy protects against epileptogenesis. Signal Transduct Target Ther 11:242. https://doi.org/10.1038/s41392-026-02738-w
42. Saadi A, Sandouka S, Grad E, Singh PK, Shekh-Ahmad T (2022) Spatial, temporal, and cell-type-specific expression of NADPH oxidase isoforms following seizure models in rats. Free Radic Biol Med 190:158–168. https://doi.org/10.1016/j.freeradbiomed.2022.08.009
43. Singh PK, Maurya S, Saadi A, Shekh-Ahmad T (2025) Targeting NOX2 mitigates seizure susceptibility, oxidative stress, and neuroinflammation in the pentylenetetrazol seizure model. Free Radic Biol Med 235:306–316. https://doi.org/10.1016/j.freeradbiomed.2025.05.386
44. Singh PK, Maurya S, Saadi A, Zhang T, Lieb A, Shekh-Ahmad T (2025) Selective inhibition of NOX2 after status epilepticus attenuates epileptogenesis and cognitive impairment: a sex-dependent study. Redox Biol 86. https://doi.org/10.1016/j.redox.2025.103830
45. Singh PK, Saadi A, Sheeni Y, Shekh-Ahmad T (2022) Specific inhibition of NADPH oxidase 2 modifies chronic epilepsy. Redox Biol 58. https://doi.org/10.1016/j.redox.2022.102549
46. Kumar Singh P, Shekh-Ahmad T (2024) Nrf2 as a potential target for the treatment of epilepsy. Neural Regen Res 19:1865–1871. https://doi.org/10.4103/1673-5374.390975
47. Sandouka S, Singh PK, Saadi A, Taiwo RO, Sheeni Y, Zhang T et al (2023) Repurposing dimethyl fumarate as an antiepileptogenic and disease-modifying treatment for drug-resistant epilepsy. J Transl Med 21:800. https://doi.org/10.1186/s12967-023-04695-2
48. Xiang L, Zhang J, Wu Y, Shi J, Shu Y, Miu R et al (2026) CHBP-loaded mesoporous polydopamine nanoparticles attenuate neuroinflammation and reprogram microglia-neuron crosstalk for spinal cord injury repair. Chem Eng J 542. https://doi.org/10.1016/j.cej.2026.177692
49. Zhang J, Xiang L, Cai X, Geng Y, Wu Y, Shi J et al (2026) 3D-MSCs apoptotic bodies-integrated conductive hydrogel mitigates spinal cord injury via immunoregulation and alleviating neuronal pyroptosis. Bioact Mater 60:704–723. https://doi.org/10.1016/j.bioactmat.2026.01.043
50. Jiang Z, Wu Z, Jin Y, Xu K, Shu W, Wu Y et al (2026) Astragaloside IV enhances autophagy to suppress endoplasmic reticulum stress and pyroptosis after spinal cord injury. Cell Signal 145. https://doi.org/10.1016/j.cellsig.2026.112571
51. Chen Y, Wang Y, Fang N, Xu J, Teng Y, Wang K et al (2026) SGK1 inhibition supports neuroprotection in spinal cord injury by suppressing oxidative stress and AIM2 activation via FoxO1 mediated mitophagy. J Neuroinflammation 23. https://doi.org/10.1186/s12974-026-03844-w
52. Wang Y, Fang N, Wang Y, Geng Y, Li Y (2024) Activating MC4R promotes functional recovery by repressing oxidative stress-mediated AIM2 activation post-spinal cord injury. Mol Neurobiol 61:6101–6118. https://doi.org/10.1007/s12035-024-03936-9
53. Basu A, Krady JK, Levison SW (2004) Interleukin-1: a master regulator of neuroinflammation. J Neurosci Res 78:151–156. https://doi.org/10.1002/jnr.20266
54. Rogove AD, Tsirka SE (1998) Neurotoxic responses by microglia elicited by excitotoxic injury in the mouse hippocampus. Curr Biol 8:19–25. https://doi.org/10.1016/S0960-9822(98)70016-8
55. Frakes AE, Ferraiuolo L, Haidet-Phillips AM, Schmelzer L, Braun L, Miranda CJ et al (2014) Microglia induce motor neuron death via the classical NF-κB pathway in amyotrophic lateral sclerosis. Neuron 81:1009–1023. https://doi.org/10.1016/j.neuron.2014.01.013

Authors and Affiliations

Volkan Gorgulu[1,2] · Cansin Sirin Tomruk[2,3] · Pelin Ergun[4,5] · Berrin Ozdil[2,6] · Ebru Sanci[7] · Aylin Buhur[2,8] · Eser Y. Sozmen[9] · Timur Kose[10] · Nefise Ulku Karabay Yavasoglu[11] · Altug Yavasoglu[2]

✉ Altug Yavasoglu
altug.yavasoglu@ege.edu.tr

Volkan Gorgulu
volkangorgulu91@gmail.com

Cansin Sirin Tomruk
cansinsirin@gmail.com

Pelin Ergun
pergun@mcw.edu

Berrin Ozdil
berrin.ozdil.bay@ege.edu.tr

Ebru Sanci
ebruusanci@gmail.com

Aylin Buhur
aylin.buhur@galata.edu.tr

Eser Y. Sozmen
esersoz@yahoo.com

Timur Kose
timur.kose@ege.edu.tr

Nefise Ulku Karabay Yavasoglu
ulku.karabay@ege.edu.tr

[1] Assisted Reproductive Treatment Center, Cam and Sakura City Hospital, Istanbul, Turkey

[2] Department of Histology and Embryology, Faculty of Medicine, Ege University, Izmir, Turkey

[3] Department of Toxicology, Sia Analysis Laboratories, Izmir, Turkey

[4] Department of Otolaryngology and Communication Sciences, Medical College of Wisconsin, Milwaukee, USA

[5] Department of Medical Biochemistry, Faculty of Medicine, Ege University, Izmir, Turkey

[6] Department of Biophysics, Faculty of Medicine, Ege University, Izmir, Turkey

[7] Center for Drug Research & Development and Pharmacokinetics Applications, Ege University, Izmir, Turkey

[8] Department of Basic Sciences, Faculty of Dentistry, Istanbul Galata University, Istanbul, Turkey

[9] Department of Medical Biochemistry, Faculty of Medicine, Tınaztepe University, Izmir, Turkey

[10] Department of Biostatistics, Faculty of Medicine, Ege University, Izmir, Turkey

[11] Department of Biology, Faculty of Science, Ege University, Izmir, Turkey